Computational Studies on Chiral Discrimination Mechanism of Phenylcarbamate Derivatives of Cellulose

Chiyo Yamamoto, Eiji Yashima,# and Yoshio Okamoto*

Department of Applied Chemistry, Graduate School of Engineering, Nagoya University, Chikusa-ku, Nagoya 464-8603

(Received December 18, 1998)

The calculations of interaction energies between cellulose tris(phenylcarbamate) (CTPC) or cellulose tris(3,5-dimethylphenylcarbamate) (CDMPC) and *trans*-stilbene oxide (**1**) or benzoin (**2**) were performed by various methods. The purpose was to gain insight into the mechanism for the chiral recognition on phenylcarbamate derivatives of cellulose which are useful chiral stationary phases for HPLC. The calculations were roughly divided into two methods: 1) Enantiomers were generated around the NH proton and the C=O oxygen of the carbamoyl group of CTPC and CDMPC which are considered to be the most important adsorption sites, and then the interaction energy was calculated. 2) Enantiomers were randomly generated by the Monte Carlo method on the surface of CTPC and CDMPC, and then the interaction energy was calculated. The results of both calculations were in good agreement with the results in the chromatographic resolution of **1** and **2** by CTPC and CDMPC.

Since optically active compounds have recently aroused wide interest in many fields dealing with pharmaceuticals, natural products, agrochemicals, and ferroelectric liquid crystals, better understanding of chiral recognition at a molecular level is of increasing importance. Moreover, chiral recognition plays an essential role in the field of enantioseparation. Chromatographic enantioseparations, particularly by high-performance liquid chromatography (HPLC), have significantly advanced in the past two decades, and are now generally recognized in many fields as one of the most powerful methods available for obtaining both pure enantiomers and for determining enantiomer composition.[1—5] The preparation of chiral stationary phases (CSPs) capable of effective chiral recognition is the key to this separation technique. Many CSPs for HPLC have been prepared. They can be classified into two types. One consists of a chiral small molecule bound to a support silica gel, and the second is derived from a chiral polymer. A great number of the former type of CSPs have been prepared, and the elucidation of the chiral discrimination mechanism on the CSPs has been attempted using spectroscopic[6—12] and computational methods.[13—17] Cyclodextrin-based CSPs[15—18] and Pirkle-type CSPs[10,11,19—21] are among the most intensively studied CSPs. Some explanatory models of interactions between the CSPs and enantiomers have been proposed on the basis of the X-ray analysis[22,23] and the solution NMR experiments including NOE studies. Computer simulations involving molecular mechanics (MM) and molecular dynamics (MD) are also applied to calculate the interaction energies between the CSPs and enantiomers. Especially, Lipkowitz et al. have been extensively studying the mechanism for the chiral recognition from theoretical viewpoints.[13—17]

Macromolecules such as proteins, polysaccharide derivatives, and synthetic chiral polymers have also been used as polymeric CSPs to separate a wide range of racemates; many polymeric CSPs are now commercially available.[1—5] However, in contract to the small molecule CSPs, the chiral recognition mechanism on the polymeric CSPs is still obscure, probably because the chiral polymers usually have a number of different binding sites with different affinities to enantiomers and the determination of their exact structures in both solid and solution is not easy.

Phenylcarbamate derivatives of polysaccharides such as cellulose and amylose are among the most useful polymeric CSPs.[3,4] They can separate a broad range of enantiomers and can give practically useful HPLC columns when they are coated on macroporous silica gel. The chiral recognition mechanism at a molecular level on the polysaccharide-based CSPs is still unclear except for a few cases, although the most important adsorbing site for chiral recognition has been considered to be the carbamate residues on the basis of the chromatographic enantioseparation results. NMR spectroscopy is a very powerful tool for understanding the nature of chiral discrimination occurring in solution, as reported for small molecule CSPs.[6—12] However, most phenylcarbamates of the polysaccharides with a high resolving ability are soluble only in polar solvents such as acetone, pyridine, and THF. In these polar solvents the derivatives show poor chiral recognition, because the solvents preferentially interact with the polar carbamate residues.[24] Therefore, it was difficult to elucidate the mechanism for discrimination between enantiomers by NMR spectroscopy in these solvents. However, we recently found that several phenylcarbamate derivatives, for instance tris(4-trimethylsiliyphenylcarbamate) (CTSP)[25,26] and tris(5-

Present address: Department of Molecular Design and Engineering, Graduate School of Engineering, Nagoya University, Chikusa-ku, Nagoya 464-8603.

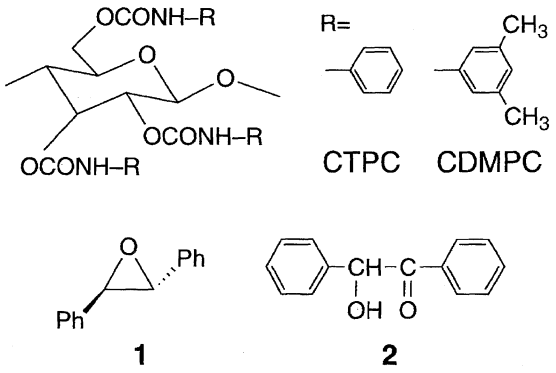

Fig. 1. Structures of cellulose phenylcarbamate derivatives (CTPC and CDMPC) and racemates (**1** and **2**).

fluoro-2-methylphenylcarbamate) (CFMPC)[27] of cellulose, are soluble in chloroform, and discriminate enantiomers in ^{1}H and ^{13}C NMR spectroscopies as well as in HPLC. In the ^{1}H NMR of *trans*-stilbene oxide (**1**), the methine protons of the oxirane ring are enantiomerically discriminated to show a set of two peaks in the presence of CTSP in $CDCl_3$. The competition experiments using acetone suggest that **1** may be adsorbed on the NH proton of the carbamate residues of CTSP.[26] These NMR studies also indicate that the most important adsorbing sites for effective chiral separation are the carbamate residues, which can interact with enantiomers mainly through hydrogen bonding. CFMPC also exhibits a high chiral recognition ability for [1,1′-binaphthalene]-2,2′-diol in NMR as well as in HPLC, and the hydroxy and some aromatic protons and carbon resonances of [1,1′-binaphthalene]-2,2′-diol are clearly separated into a pair of peaks due to enantiomers in the presence of CFMPC in NMR. Therefore, the binding geometry and dynamics between CFMPC and the enantiomers could be investigated on the basis of spin-lattice relaxation time, ^{1}H NMR titrations, and intermolecular NOEs in the presence of CFMPC, and a model for the complex could be proposed. This permitted us, for the first time, to investigate the chiral interaction occurring in solution by NMR spectroscopy.[27] However, most phenylcarbamates of the polysaccharides with high resolving ability are soluble only in polar solvents, as described previously. For such $CDCl_3$-insoluble phenylcarbamate derivatives of polysaccharides, a computer simulation involving MM and MD calculations will be a useful and effective approach for elucidating the mechanism for the chiral recognition and for predicting the elution order of enantiomers.

In this paper, we report computational studies on the chiral discrimination mechanism of CTPC and CDMPC (Fig. 1), which are commercially available CSPs for HPLC. Especially, among the tris(phenylcarbamate) derivatives of cellulose so far prepared, CDMPC shows excellent resolving ability for a variety of racemates and is used as one of the most popular CSPs in the world. The structures of CTPC and CDMPC were constructed on the basis of X-ray analysis data of CTPC. As racemates, *trans*-stilbene oxide (**1**) and benzoin (**2**) were selected (Fig. 1). **1** has an ether oxygen capable of hydrogen bonding and can be completely separated by HPLC on CTPC and CDMPC with inversion in elution order, while **2** can be resolved on CDMPC, but not resolved on CTPC. These chromatographic results were simulated with computational calculations using various methods.

Experimental

Computational Method. MM and MD calculations were performed with three forcefields; CHARMm forcefield[28–30] as implemented in Quanta/CHARMm program[31] (ver 4.0, Molecular Simulations Inc., Burlington, MA), Dreiding forcefield (version 2.1.1)[32] as implemented in CERIUS^2 software (version 1.6, MSI),[33] and pcff forcefield[34–36] available with the Discover software (version 4.0.0, MSI)[37] running on an Indigo^2-Extreme and an Indigo^2-Impact work station (Silicon Graphics). Charges on atoms were calculated using Charge Equilibration (QEq) method[38] in CERIUS^2; total charges of the molecules were zero.

The calculated total energies (E) in each forcefield are expressed in the forms

$$E = E_{\text{bond length}} + E_{\text{bond angle}} + E_{\text{dihedral angle}} + E_{\text{improper torsion}} + E_{\text{electrostatic}} + E_{\text{van der Waals}} \quad \text{(CHARMm)} \tag{1}$$

$$E = E_{\text{bond length}} + E_{\text{bond angle}} + E_{\text{dihedral angle}} + E_{\text{improper torsion}} + E_{\text{electrostatic}} + E_{\text{van der Waals}} + E_{\text{H bond}} \quad \text{(Dreiding)} \tag{2}$$

$$E = E_{\text{bond length}} + E_{\text{bond angle}} + E_{\text{dihedral angle}} + E_{\text{improper torsion}} + E_{\text{cross term}} + E_{\text{electrostatic}} + E_{\text{van der Waals}} \quad \text{(pcff)} \tag{3}$$

here

$$\begin{aligned} E_{\text{cross term}} = & \sum_b \sum_{b'} F_{bb'}(b - b_0)(b' - b_0') \\ & + \sum_\theta \sum_{\theta'} F_{\theta\theta'}(\theta - \theta_0)(\theta' - \theta_0') \\ & + \sum_b \sum_\theta F_{b\theta}(b - b_0)(\theta - \theta_0) \\ & + \sum_b \sum_\phi (b - b_0)[V_1\cos\phi + V_2\cos 2\phi + V_3\cos 3\phi] \\ & + \sum_{b'} \sum_\phi (b' - b_0')[V_1\cos\phi + V_2\cos 2\phi + V_3\cos 3\phi] \\ & + \sum_\theta \sum_\phi (\theta - \theta_0)[V_1\cos\phi + V_2\cos 2\phi + V_3\cos 3\phi] \\ & + \sum_\phi \sum_\theta \sum_{\theta'} K_{\phi\theta\theta'}\cos\phi(\theta - \theta_0)(\theta' - \theta_0') \end{aligned} \tag{4}$$

where b is the bond length and b_0 is the reference value, and θ and ϕ are the bond angle and the torsion angle, respectively. Several cross-coupling terms $E_{\text{cross term}}$ are used in the pcff forcefield such as bond-bond, angle-angle, bond-angle, bond-torsion, angle-torsion, and angle-angle-torsion.

The Dreiding forcefield uses a "special" hydrogen bond potential to describe the interaction between atoms involved in hydrogen bonds.

Calculation of Interaction Energy between CTPC and Enantiomers. The interaction energies (E') in the CHARMm and pcff forcefields derived from van der Waals force and electrostatics force between an atom i and an atom j can be calculated with the following equation:

$$E' = E_{\text{electrostatic}} + E_{\text{van der Waals}} \tag{5}$$

CHARMm

$$E_{\text{electrostatic}} = \sum_{i,j>i}(q_i q_j)/(4\pi\varepsilon_0 r_{ij}) \quad (6)$$

$$E_{\text{van der Waals}} = \sum_{i,j>i}\left\{(A_{ij}/r_{ij})^{12} - (B_{ij}/r_{ij})^{6}\right\} \quad (7)$$

pcff

$$E_{\text{electrostatic}} = \sum_{i,j>i}(q_i q_j)/(\varepsilon r_{ij}) \quad (8)$$

$$E_{\text{van der Waals}} = \sum_{i,j>i}\left\{(A_{ij}/r_{ij})^{9} - (B_{ij}/r_{ij})^{6}\right\} \quad (9)$$

where q_i and q_j represent electric charge of atoms i and j, respectively, ε_0 is the effective dielectric constant, and r_{ij} is the interatomic distance computed from the Cartesian coordinates. The two nonbonded parameters A_{ij} and B_{ij} are derived from the atom polarizabilities and the effective number of outer shell electrons.

In the Dreiding forcefield, the hydrogen bond (H bond) potential is one of components of interaction energy (E').

$$E' = E_{\text{electrostatic}} + E_{\text{van der Waals}} + E_{\text{H bond}} \quad (10)$$

$$E_{\text{electrostatic}} = C_0 \sum_{i,j>i}(q_i q_j)/(\varepsilon r_{ij}) \quad (11)$$

$$E_{\text{van der Waals}} = \sum_{i,j>i}\left[D_0\left\{(r_{0ij}/r_{ij})^{12} - 2(r_{0ij}/r_{ij})^{6}\right\}\right] \quad (12)$$

$$E_{\text{H bond}} = \sum_{i,j>i}\left[D_0\left\{5(r_{0ij}/r_{ij})^{12} - 6(r_{0ij}/r_{ij})^{10}\right\}\right] \quad (13)$$

where ε is the dielectric constant ($\varepsilon = 1$ for a vacuum) and the conversion factor (C_0) is 332.0637. R_0 and D_0 are the bond length and bond strength (well depth), respectively.

Interaction energies were calculated by four methods based on three programs supplied by MSI, which were used as such or modified as below.

Method I. Molecular Interaction program in Quanta was used with the CHARMm forcefield. The detailed calculation method was already reported.[39] First, a center of a cubic sampling box is placed on an atom i of CTPC. Here, the size of the cubic sampling box is specified as r, and the mesh size is specified as r'. Then, each enantiomer is placed at a grid point and is allowed to rotate from 0° to 360° along the x, y, and z axes individually at angle intervals (ω_x, ω_y, ω_z). The interaction energies are calculated for a given set of grid points and (ω_x, ω_y, ω_z).

Method II. The Blends program in CERIUS[2] which was developed to calculate the compatibility of binary mixtures ranging from small molecules to large macromolecular systems based on a modified Flory–Huggins[40] was applied to calculate interaction energies with the Dreiding forcefield. The program uses the Monte Carlo atomistic simulations both to generate thousands of different molecular orientations and to calculate their pair-interaction energies.[41] This approach generates energetically favorable configurations by employing a Monte Carlo technique that includes excluded-volume constraints. The procedure used in this study (Fig. 2) includes the following steps;[42]

Step 1. Structures of each enantiomer and CTPC or CDMPC are constructed and optimized. The overall shape of each molecule is represented by its van der Waals surface.

Step 2. The centers of mass of both molecules are positioned near the origin of the Cartesian coordinate frame, while the coordinates of molecule 1 (CTPC or CDMPC, white in Fig. 2) are unchanged during the calculations.

Step 3. A particular orientation of molecule 2 (an enantiomer, gray in Fig. 2) is selected randomly using three Euler angles.

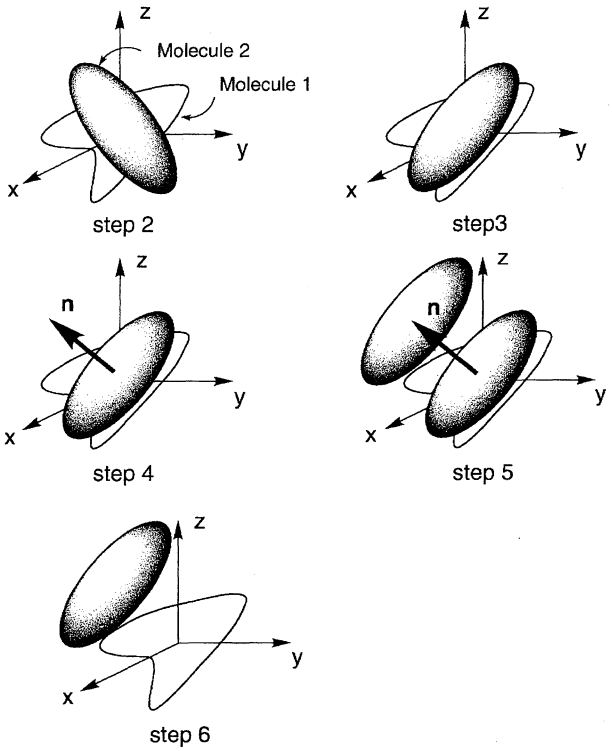

Fig. 2. Consecutive steps for a calculation of the pair energy of a single configuration. Details are available in the text.

Step 4. A vector ($\boldsymbol{n}$) that points from the origin to the surface of a unit sphere is randomly chosen.

Step 5. Molecule 2 is translated along the vector determined by Step 4 until the van der Waals surfaces of each molecule just touch each other.

Step 6. The interaction energy between the molecules is calculated and stored.

Step 7. Steps 3 through 6 are repeated a specified number of times.

Method III. The modified Blends program was used. The details are described in Results and Discussion.

Method IV. The Flexiblend module[43] in Insight II/Discover was employed; this has been used for the rapid estimation of polymer miscibility. First, two molecules are placed with their centers of mass coincident, and are randomly oriented in space, and then positioned relative to each other using the Slide Together method: The molecules are initially placed far from one another and moved together by given increments. The intermolecular energy is evaluated at each step. If at a given step the energy exceeds the given energy limit, one step back is taken, and if the energy is then below the limit, the resulting structure is accepted as a starting configuration. The starting configurations are relaxed by MM energy minimization. The procedure is repeated until a specified number of configurations (1000) is obtained.

Results and Discussion

Coordinates of Racemates and Polysaccharides. The initial structure of the (*R,R*)-(+)-**1** was constructed by the MM calculations. The energy minimization of the obtained structure was performed by using Conformational Search in CERIUS[2]. The energy minimization was accomplished by Conjugate Gradient 200 (CG200) until the root mean

square (rms) value became less than 0.1 kcal mol^{-1} Å^{-1} or 500 steps of the minimization are performed. Four lowest-energy structures were extracted and further minimizations (rms 0.01 kcal mol^{-1} Å^{-1}) were performed by CG 200 and Fletcher Powell (FP) on each structure. However, significant differences in energy among four structures were not detected. The most symmetrical structure was adopted. The (*S,S*)-(−)-**1** was constructed as that of the (*R,R*)-(+)-**1**.

The initial atomic coordinates of the (*R*)-(−)-**2** were taken from the crystal structure data[44] in the Cambridge Structural Database 3D Graphics Search System[45] and the structure was further energy minimized with CG 200 and FP using the Dreiding force field until the rms value became less than 0.01 kcal mol^{-1} Å^{-1}. The (*S*)-(+)-**2** was constructed as that of the (*R*)-(−)-**2**.

The polymer model of CDMPC was constructed using the structure of CTPC postulated on the basis of X-ray analysis according to the previously reported method with a modification.[27,39] First, a full energy minimization of a repeating unit of CDMPC containing CH_3O groups at the 1- and 4-positions of a glucose unit, was performed using the Conformational Search in CERIUS^2. The energy minimization was done first by CG 200 and then FP until the rms value became less than 0.01 kcal mol^{-1} Å^{-1}. Next, the monomeric units of CDMPC were allowed to construct a trimer with left-handed 3-fold (3/2) helix by Polymer Builder in CERIUS^2 according to the structure of CTPC.[46] The trimer was placed into a simulation cell ($x = 40$, $y = 40$, and $z = 14.441$ Å) under three-dimensional periodic boundary conditions by Crystal Builder in CERIUS^2. The unit cell volume was expanded to the directions perpendicular to the polymer axis (z) to avoid interactions between the periodic polymer and neighboring ones in other cells. The energy minimization was then accomplished by CG 200 and FP until the rms value became less than 0.01 kcal mol^{-1} Å^{-1}, respectively. The MD calculation was applied to the optimized trimer in the cell at 300 K for 10 ps with a step size of 1 fs using Constant NVT (HOOVER) method. The structures with lower energies were extracted from the trajectory files and the MM calculations as described above were performed for these ex-

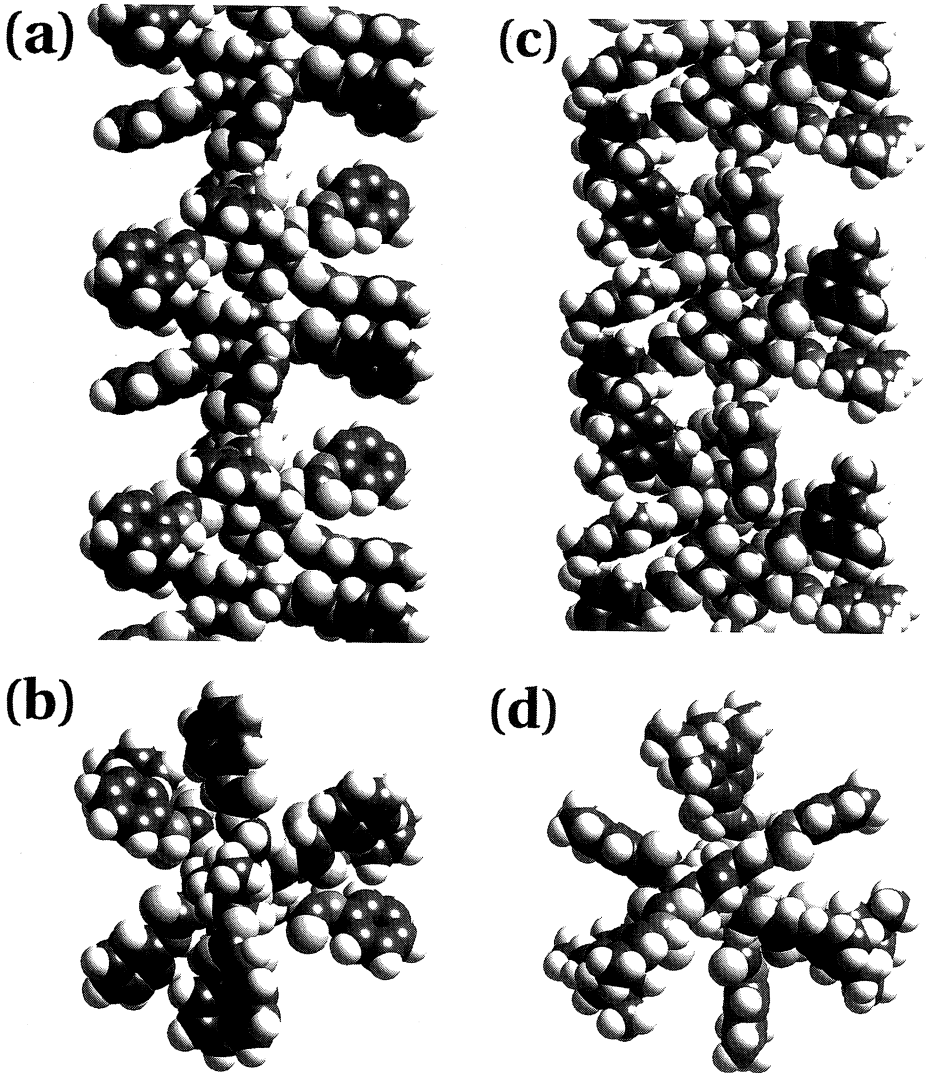

Fig. 3. Optimized structures of CTPC (a and b) and CDMPC (c and d). Perpendicular to the chain axis (a and c) and along to the chain axis (b and d).

tracted structures again. The resulting optimized trimer with the most symmetrical structure in the unit cell was connected to give a nanomer (9mer) as the model polymer of CDMPC.

A repeating unit of CTPC was obtained by replacement of the methyl groups on the phenyl group of CDMPC with protons. The polymer model of CTPC was constructed and optimized in the same way as that for CDMPC. The structures of CTPC and CDMPC are shown in Fig. 3. The optimized structures of CTPC and CDMPC have a similar left-handed 3/2 helix and the glucose residues are regularly arranged along the helical axis. A chiral helical groove with polar carbamate groups exists along the main chain. The polar carbamate groups are preferably located inside, and hydrophobic aromatic groups are placed outside the polymer chain so that polar enantiomers may predominantly interact with the carbamate residues in the groove through hydrogen-bond formation. Both structures are similar, but the aromatic rings of CDMPC are arranged differently parallel to the helical axis, probably due to the steric hindrance of the methyl groups on the phenyl moiety. This may be responsible for the reversed enantioselectivity of CTPC and CDMPC toward some racemates.

Calculation of Interaction Energies between CTPC or CDMPC and Enantiomers. Figure 4 shows chromatograms of the resolution of racemic **1** and **2** on HPLC columns packed with CTPC and CDMPC. Racemic **1** is completely resolved on CTPC ($\alpha = 1.46$) and CDMPC ($\alpha = 2.42$). However, the order of elution is reversed; the (*R,R*)-(+)-isomer eluted first followed by the (*S,S*)-(−)-isomer on CTPC, whereas the (*S,S*)-(−)-isomer eluted first on CDMPC. Racemic **2** is completely resolved on CDMPC ($\alpha = 1.58$), but not separated on CTPC ($\alpha \approx 1$).

The methods used for calculating the interaction energy are roughly divided into two types, which differ in the way to generate enantiomers. In Method I, enantiomers were generated around the NH protons or C=O oxygens of the carbamoyl group of CTPC and CDMPC, which are considered to be the most important adsorption sites for **1** or **2**. On the other hand, in Methods II, III, and IV, enantiomers were randomly generated by the Monte Carlo method on the surface of CTPC or CDMPC molecule. The calculation results using these methods are described below.

Method I. In the case of **1**, the cyclic ether oxygen may interact with the NH proton of the carbamate residue through hydrogen bonding. Therefore, a center of a cubic sampling box ($r = 4$ Å) was placed on the NH proton, then the mesh size ($r' = 0.5$ Å) was specified, and at each grid point each enantiomer was rotated at 15° intervals for the x, y, and z axes, individually (Fig. 5a). The size of the sampling boxes ($r = 4$ Å) is suitable for the calculation of the interaction energy.[39] The calculation was carried out at each NH proton at the 2-, 3-, and 6-positions of glucose units of 4, 5, and 6 in order to avoid the influence of the end-groups, since CTPC used as the CSP is a polymer with degree of polymerization ≈ 200 (Fig. 5b). In the case of **2**, the hydroxy proton and/or the C=O oxygen of **2** may interact with the C=O oxygen and the NH proton of the carbamate residue, respectively, and therefore, a center of a cubic sampling box was placed on the NH proton and the C=O oxygen. The calculation results were evaluated with the lowest interaction energy and the distribution of the interaction energy.

The results of the calculations for CTPC and **1** are shown

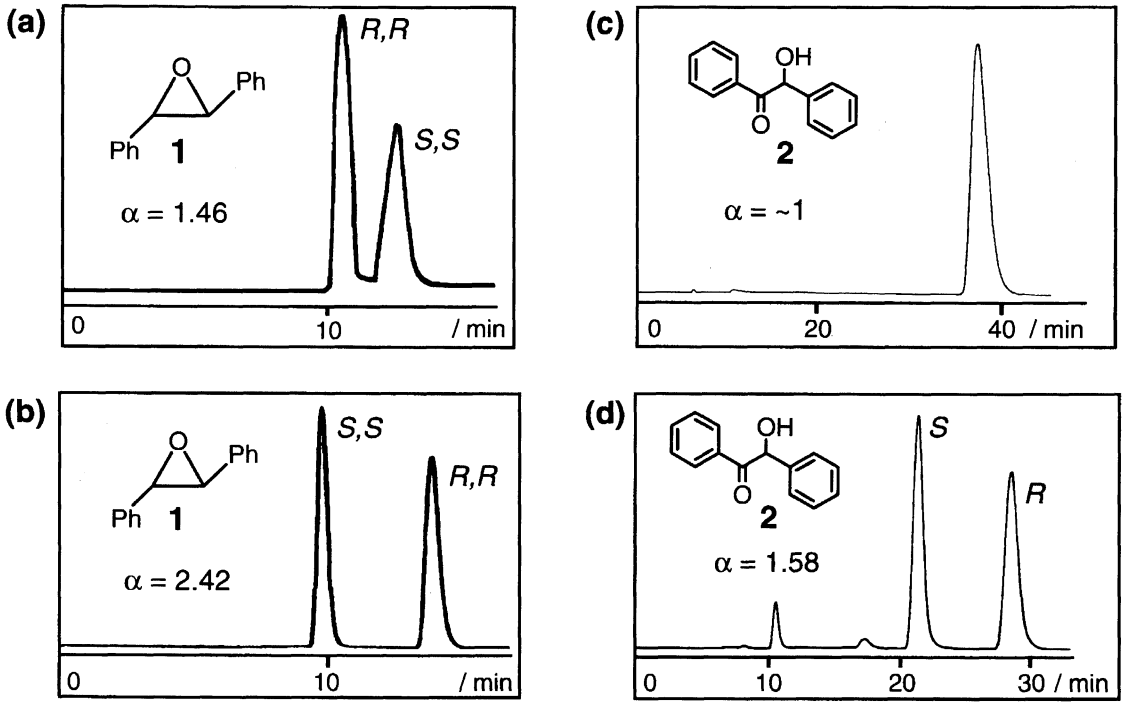

Fig. 4. Chromatograms of the enantioseparation of **1** and **2** on CTPC (a and c) and CDMPC (b and d) with hexane-2-propanol (90/10) as the eluent. Columns, 25×0.46 (i.d.) cm; flow rate, 0.5 ml min^{-1}.

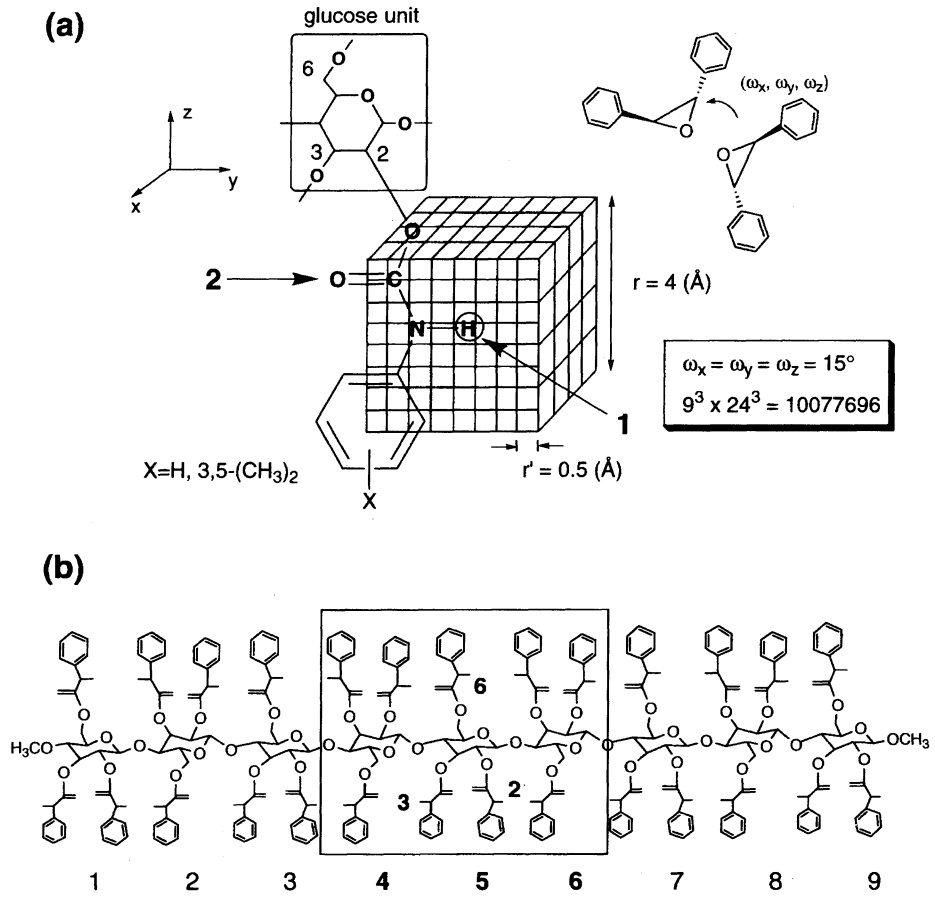

Fig. 5. Method of calculation of interaction energy between CTPC or CDMPC and enantiomers of **1** or **2** (a). Nanomer of CTPC (b).

in Table 1. The interaction energies between CTPC and the (*S,S*)-(−)-**1** were lower than those between CTPC and the (*R,R*)-(+)-**1** except on 4-6 (6-position at glucose unit No. 4) and 6-2. Figure 6a shows the distribution of the interaction energy. The number of the interaction energies for the (*S,S*)-(−)-**1** under 100 kcal mol^{-1} was more than that for the (*R,R*)-(+)-**1**. These data suggest that the (*S,S*)-(−)-**1** may more strongly interact with the CTPC than the (*R,R*)-(+)-**1**. The calculation results for CDMPC and **1** are also presented in Table 1 and Fig. 6b. Most of the lowest interaction energies between CDMPC and **1** were larger than those between CTPC and **1**, and all interaction energies on 3-position were over 100 kcal mol^{-1}. However, the interaction energies between CDMPC and the (*R,R*)-(+)-**1** were lower than those between CDMPC and the (*S,S*)-(−)-**1** except on 4-6, and the distribution of the interaction energies also indicates the (*R,R*)-(+)-**1** preference.

In the case of CTPC and **2**, the lowest energy at the NH proton was observed for the (*R*)-(−)-isomer, whereas the lowest energy at the C=O oxygen was observed for the (*S*)-(+)-isomer (Table 2). The differences of the lowest energies between the (*R*)-(−)- and the (*S*)-(+)-isomer at the same position are relatively small. Moreover, in the distribution of interaction energy under 100 kcal mol^{-1}, there is not a significant difference between the (*R*)-(−)- and the (*S*)-(+)-isomer (Figs. 7a and 7b). However, the number of interaction energies less than 100 kcal mol^{-1} at the C=O oxygen is more than those at the NH proton. This means that the main interaction sites for **2** seems to be the C=O oxygen of the carbamate residue of CTPC. In the chromatographic resolution of **2** using CTPC as a CSP, the enantiomers are not resolved ($\alpha \approx 1$), and therefore, the calculation results are in agreement with the observed chromatographic resolution on CTPC. In the case of CDMPC and **2**, there is no significant difference in the lowest interaction energies between the (*R*)-(−)- and the (*S*)-(+)-isomer (Table 2), whereas a clear difference in number of the interaction energy under 100 kcal mol^{-1} at the C=O was observed (Figs. 7c and 7d). These results indicate that the interaction at the C=O oxygen may contribute to discriminate the enantiomers of **2**; the calculation results appear to agree with the chromatographic enantioseparation result (Fig. 4(d)).

Method II. In this method, each enantiomer with a particular orientation was randomly generated one million times on the surface of a CTPC or a CDMPC molecule defined by a specific van der Waals radius in the Dreiding force field and the interaction energies between CTPC or CDMPC and **1** or **2** for each combination and the average interaction energy were calculated. To avoid the influence of the end-groups, enantiomers were generated on the surface of the middle part of CTPC and CDMPC. The results are summarized in Table 3. The averaged interaction energies for the two enantiomers (**1** and **2**) were almost equal, while a slight difference in the energy was observed for the average

Table 1. The Lowest Interaction Energy (kcal mol^{-1}) between CTPC or CDMPC and **1** Calculated by Method I[a)]

Glucose no.	CTPC		CDMPC	
and position	(*R*,*R*)-(+)-**1**	(*S*,*S*)-(−)-**1**	(*R*,*R*)-(+)-**1**	(*S*,*S*)-(−)-**1**
4-2	−5.49	−23.6	62.8	77.0
4-3	−18.9	−42.0	—[b)]	—
4-6	−47.4	−44.0	−13.0	−16.6
5-2	−22.6	−27.2	−8.02	−5.86
5-3	−15.1	−37.3	—	—
5-6	−39.6	−44.0	40.1	53.0
6-2	−16.1	−14.1	−29.5	−24.8
6-3	−21.4	−36.8	—	—
6-6	−36.2	−41.4	−5.34	12.1

a) r = 4 Å, r' = 0.5 Å, ω_x, ω_y, and ω_z = 15°, see text. b) Dashes indicate over 100 kcal mol^{-1} (1 cal = 4.184 J).

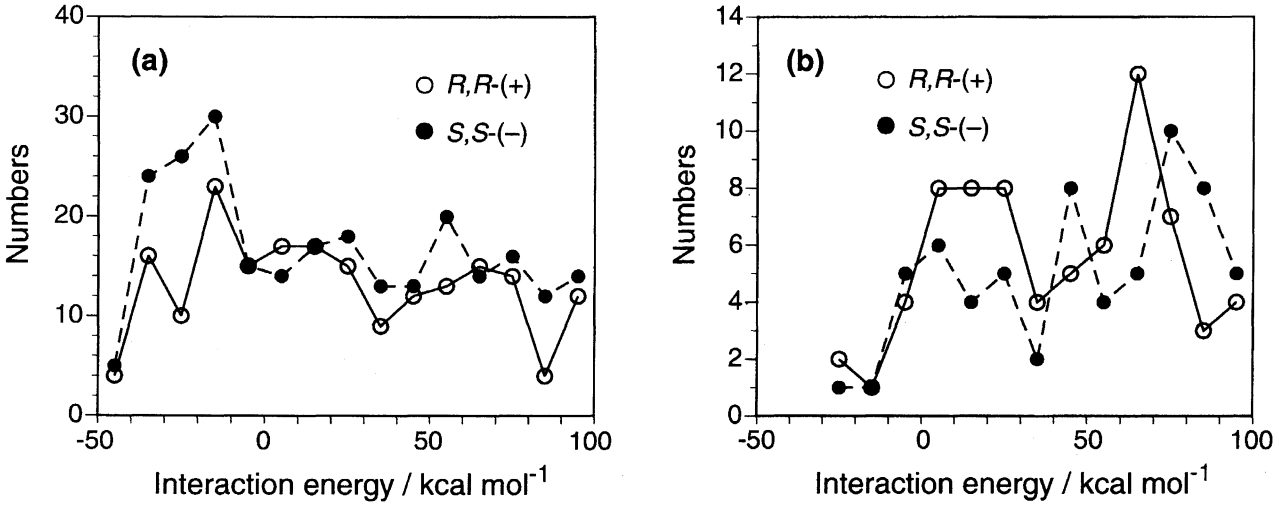

Fig. 6. Distribution of interaction energy under 100 kcal mol^{-1} between CTPC and (*R*,*R*)- or (*S*,*S*)-**1** (a); between CDMPC and (*R*,*R*)- or (*S*,*S*)-**1** (b).

Table 2. The Lowest Interaction Energy (kcal mol^{-1}) between CTPC or CDMPC and **2** at NH or C=O Positions Calculated by Method I[a)]

Glucose no.	CTPC				CDMPC			
	N–H		C=O		N–H		C=O	
and position	(*R*)-(−)-**2**	(*S*)-(+)-**2**	(*R*)-(−)-**2**	(*S*)-(+)-**2**	(*R*)-(−)-**2**	(*S*)-(+)-**2**	(*R*)-(−)-**2**	(*S*)-(+)-**2**
4-2	17.7	9.00	−12.3	−15.7	15.8	62.5	93.4	76.6
4-3	−39.0	−35.4	−33.4	−37.4	11.3	−3.19	11.9	8.52
4-6	−39.4	−35.9	−27.9	−29.5	−27.5	−25.7	−27.1	−29.5
5-2	−27.9	−23.8	−29.0	−34.2	7.38	52.2	20.0	18.7
5-3	−45.8	−34.4	−37.3	−40.1	—[b)]	41.6	−30.1	−10.7
5-6	−41.2	−40.6	−32.0	−29.6	32.4	36.7	−23.5	−31.0
6-2	−30.6	−28.4	−33.0	−33.1	27.1	39.4	55.1	48.2
6-3	−28.0	−28.0	−38.0	−41.9	—	—	−29.8	−25.4
6-6	−32.0	−38.0	−33.8	−30.4	−5.91	−16.8	−28.1	−26.2

a) r = 4 Å, r' = 0.5 Å, ω_x, ω_y, and ω_z = 15°, see text. b) Dashes indicate over 100 kcal mol^{-1} (1 cal = 4.184 J).

of the lowest 20 interaction energies. However, this difference is smaller than the expected energy difference from the observed chiral HPLC results. The computer graphics of the interaction between the CTPC and the (*S*,*S*)-(−)-**1** with the lowest energy is shown in Fig. 8. Both enantiomers exist on outside of CTPC surface, far from the carbamoyl residue inside the CTPC. This means that the enantiomers can not interact with the carbamoyl groups, which must be the most important sites for efficient chiral discrimination. Consequently, this method is not suitable for simulating the chromatographic enantioseparation results.

Method III. On the basis of the above results, we con-

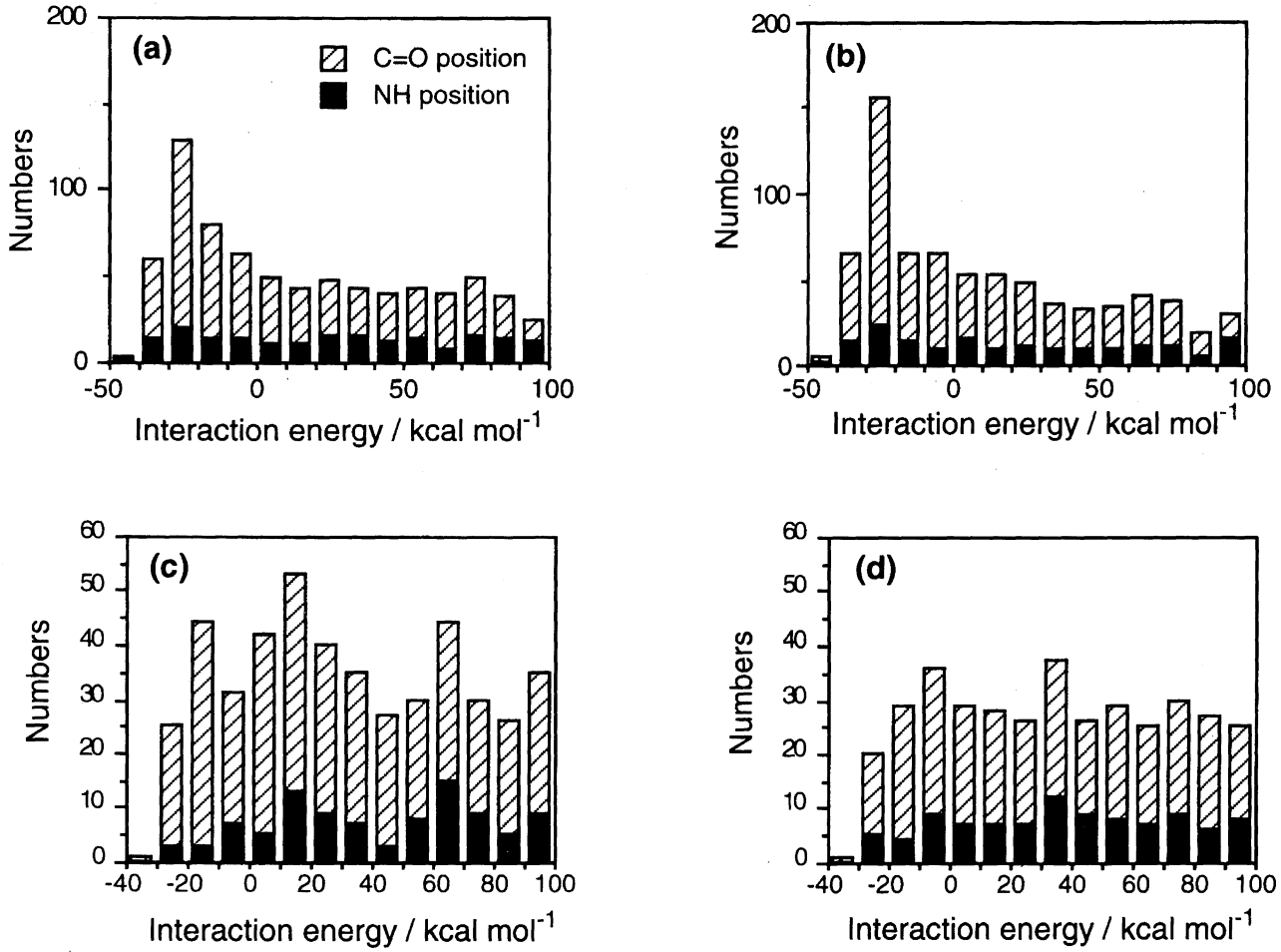

Fig. 7. Distribution of interaction energy under 100 kcal mol^{-1} between CTPC and (*S*)-(a) and (*R*)-**2** (b); between CDMPC and (*S*)- (c) and (*R*)-**2** (d) at the C=O and the N–H positions.

Table 3. Interaction Energies (kcal mol^{-1}) Calculated by Method II and the Free Energy Difference Estimated by Chiral HPLC.

	CTPC and **1**		CDMPC and **1**		CTPC and **2**		CDMPC and **2**	
	(*R*,*R*)-**1**	(*S*,*S*)-**1**	(*R*,*R*)-**1**	(*S*,*S*)-**1**	(*R*)-**2**	(*S*)-**2**	(*R*)-**2**	(*S*)-**2**
Total[a)]	−1.24	−1.24	−1.14	−1.14	−1.21	−1.22	−1.14	−1.15
Av. Lowest 20[b)]	−9.88	−9.87	−8.80	−8.53	−12.0	−12.2	−9.30	−9.22
$-\Delta\Delta G$ (kcal mol^{-1})[c)]	0.23 (*S*,*S*)		0.53 (*R*,*R*)		ca. 0		0.27 (*R*)	

a) The averaged interaction energies for one million combinations of CTPC or CDMPC and **1** or **2**. b) The average of the lowest 20 interaction energies. c) The difference in free energy ($-\Delta\Delta G$). $-\Delta\Delta G$ was estimated by the enantioseparation factor (α) using the equation, $\Delta\Delta G = -RT\ln\alpha$,where R and T are the gas constant (1.987 cal mol^{-1} K^{-1}) and the absolute temperature in K, respectively. The configuration of the more retained enantiomer is shown in parentheses.

sidered that, if enantiomers could be generated inside of the polymer surface, enantiomers could interact with the carbamoyl groups, which will lead a difference in interaction energy. To achieve this strategy, Method II was modified: A downward scaling of the van der Waals radii of atoms was performed and then the radii was returned to full value with stagewise minimization. This method was developed by Suter et al., to construct models of well-relaxed amorphous glassy polymers and was called a "blowing up" technique.[47]

To generate enantiomers inside of the polymer surface, the initial van der Waals radii of atoms were reduced to 70% of their full values defined in the Dreiding force field. Each enantiomer of **1** was then randomly generated 10000 times on the surface of a CTPC molecule defined by the van der Waals radius, and these structures were stored in an energy file. This step was repeated 100 times using different random seeds (100 energy files were constructed) and the ten lowest energy structures in each energy file were selected (10 × 100). Further, a four-step "blowing up" technique described below was performed, while the geometry of CTPC was

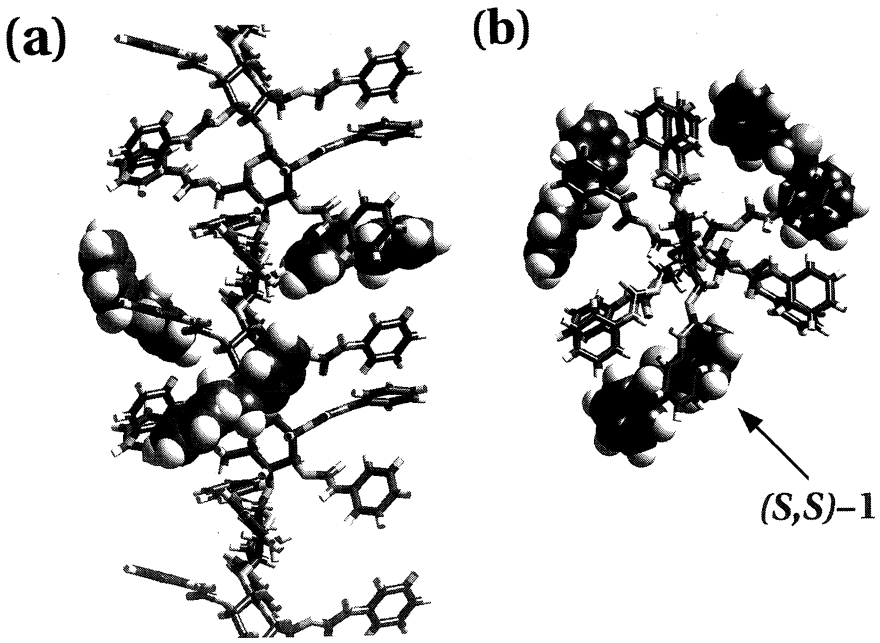

Fig. 8. Calculated structure of the CTPC–(*S,S*)-**1** complex obtained by Method II. View along the helix axis (a) and perpendicular to the helix axis (b).

fixed;

Step 1: The van der Waals radii of atoms increased to 80% of their full values and the MM calculations were performed using CG200 until the residual rms force of the structure reaches below 1.0 kcal mol^{-1} Å^{-1}.

Step 2: The van der Waals radii of atoms increased to 90% of their full values and the MM calculations were done as Step 1.

Step 3: The van der Waals radii of full values were employed and the MM calculations were performed using CG 200 until the residual rms force of the structure reaches below 1.0 kcal mol^{-1} Å^{-1}.

Step 4: Further MM calculations were performed with CG 200 until the residual rms force of the structure reaches below 0.1 kcal mol^{-1} Å^{-1}. The QEq calculations were performed every 30 steps of calculation.

The calculation results are summarized in Table 4 using the averaged and the lowest total interaction energies and their components. The sum of the averages of van der Waals, Coulomb, and H-bond forces is equal to the average of the total interaction energy. Both the averaged and the lowest interaction energies were significantly lower than those calculated by Method II, indicating the usefulness of this method and the attractive interaction between them. The interaction energy between CTPC and the (*S,S*)-(−)-**1** were lower than those between CTPC and the (*R,R*)-(+)-**1** except for minimum energy of hydrogen bond force. Figure 9 shows the computer graphics of the interaction between CTPC and the (*S,S*)-(−)-**1** with the lowest hydrogen bond energy. The (*S,S*)-(−)-**1** is bound in a chiral groove, and each phenyl group may interact with the phenyl groups of CTPC through π–π interactions; the ether oxygen atom of the (*S,S*)-(−)-**1** is located near the NH proton of CTPC and can form a hydrogen bond. Compared with the model (Fig. 8) having the lowest interaction energy in Method II, the (*S,S*)-(−)-**1** apparently gets into the inside of CTPC to form a hydrogen bonding with the NH proton of the carbamoyl group (Fig. 9).

Method IV. In this method, enantiomers were generated outside of CTPC and approached into the direction toward the chiral groove of CTPC. This method appears to reproduce the motion of an enantiomer during the actual enantioseparation by HPLC. Generation of enantiomers was performed by the Flexiblend/Slide Together algorithm.[43] Each enantiomer with a particular orientation was initially generated at a distance of 15 Å apart from the CTPC center and approached to the CTPC center by 0.2 Å steps. The intermolecular energy was evaluated at each step. If the energy exceeds the given limit energy (10^5 kcal mol^{-1}), one step back is taken, and if the energy is then below the limit, the resulting structure is considered to be an acceptable starting

Table 4. Total and Components of Interaction Energies (kcal mol^{-1}) between CTPC and **1** Calculated by Method III

	Total		VDW		Coulomb		H-bond	
	Lowest	Av.	Lowest	Av.	Lowest	Av.	Lowest	Av.
(*R,R*)-(+)-**1**	−27.10	−15.71	−21.20	−12.61	−8.36	−3.07	−3.19	−0.03
(*S,S*)-(−)-**1**	−27.67	−16.17	−21.72	−12.66	−9.19	−3.42	−2.96	−0.09

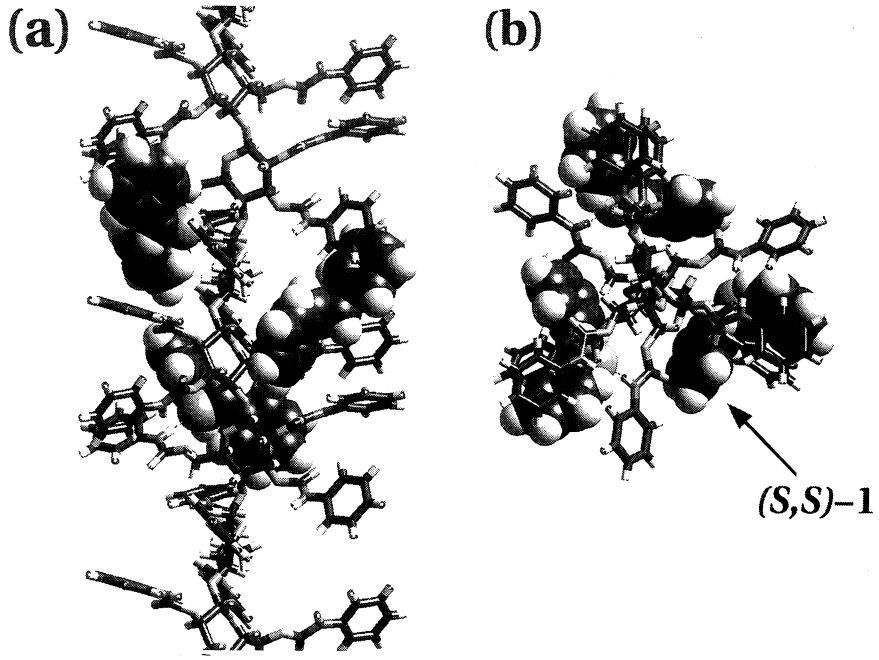

Fig. 9. Calculated structure of the CTPC–(*S,S*)-**1** complex formed through hydrogen bonds obtained by Method III. View along the helix axis (a) and perpendicular to the helix axis (b).

configuration. This procedure was repeated until 1000 configurations were obtained. The structures were relaxed by MM energy minimization, while the geometry of the CTPC was fixed. The minimization was allowed to proceed until the maximum derivatives reached below 1 kcal mol^{-1} Å^{-1}. As a result, the numbers of the total interaction energy under 100 kcal mol^{-1} between the CTPC and enantiomers of **1** were 998 for the (*R,R*)-(+)-**1** and 999 for the (*S,S*)-(−)-**1**, and the averages of them were −21.19 and −21.03 kcal mol^{-1}, respectively. This indicates that the (*S,S*)-(−)-**1** may interact more tightly with the CTPC than the (*R,R*)-(+)-**1**, which agreed well with the chromatographic resolution results.

Conclusions

The interaction energies between CTPC or CDMPC and *trans*-stilbene oxide or benzoin were calculated by using various forcefields and methods. Significant differences of interaction energies between enantiomers appeared only in the cases where enantiomers were generated inside of CTPC or CDMPC. The results indicate that the polar carbamate residues of cellulose derivatives may be the most important adsorbing site for polar racemates and may play a role in the chiral recognition.

The calculations agreed with the observed results for the chromatographic resolution on CTPC and CDMPC. The adaptability of these methods to various kinds of polysaccharides derivatives and racemates must be investigated. In this study, interactions between a single molecule of the polysaccharides and an enantiomer are taken into consideration, since polar racemates may interact preferentially with polar carbamate residues inside the polymer chain. However, besides these polar interactions, the π–π interaction between the phenyl groups of phenylcarbamate derivatives of polysaccharides and the aromatic groups of an enantiomer must play a role in the chiral recognition, because several nonpolar aromatic compounds can also be resolved.[48—50] Especially under reverse-phase conditions using aqueous eluents, hydrophobic chiral cavities between the polymer chains may play an important role for chiral discrimination. Further computational studies are required for more accurate prediction of chromatographic enantioseparation. Moreover, the use of MD calculations will be needed. However, we believe that the methods reported here are useful for a qualitative understanding of the chiral recognition mechanism of cellulose phenylcarbamates. This approach is not restricted to the study of chiral recognition and must be applicable to a variety of bimolecular interactions.

We thank Mrs. Makiko Yamada (Naruse) for her experimental support. We also acknowledge Mr. H. Shimizu (Kubota Graphics Technologies), Mr. J. Goto (Ryoka Systems Inc.), and Dr. A. Bick (MSI) for their useful technical suggestions for the use and modification of the MSI programs. This work was partially supported by Grants-in-Aid for Scientific Research on Priority Areas Nos. 08559008 and 706 (Dynamic Control of Stereochemistry) from the Ministry of Education, Science, Sports and Culture, and the Venture Business Laboratory Project "Advanced Nanoprocess Technologies" at Nagoya University. C. Y. acknowledges the support by a Grant-in-Aid for JSPS Fellows (No. 1802) from the Ministry of Education, Science, Sports and Culture.

References

1 S. Ahuja, "Chiral Separations by Liquid Chromatography," ed by S. Ahuja, ACS Symposium Series 471, Washington D. C. (1991), p. 1.

2 D. R. Taylor and K. Maher, *J. Chromatogr. Sci.*, **30**, 67 (1992).
3 Y. Okamoto and E. Yashima, *Angew. Chem., Int. Ed. Engl.*, **37**, 1020 (1998).
4 E. Yashima, C. Yamamoto, and Y. Okamoto, *Synlett*, **1998**, 344.
5 W. H. Pirkle and T. C. Pochapsky, *Chem. Rev.*, **89**, 347 (1989).
6 B. Feibush, A. Figueroa, R. Charles, K. D. Onan, P. Feibush, and B. L. Karger, *J. Am. Chem. Soc.*, **108**, 3310 (1986).
7 W. H. Pirkle and T. C. Pochapsky, *J. Am. Chem. Soc.*, **109**, 5975 (1987).
8 G. U.-Barretta, C. Rosini, D. Pini, and P. Salvadori, *J. Am. Chem. Soc.*, **112**, 2707 (1990).
9 K. B. Lipkowitz, S. Raghothama, and J. Yang, *J. Am. Chem. Soc.*, **114**, 1554 (1992).
10 W. H. Pirkle and C. J. Welch, *J. Chromatogr. A.*, **683**, 347 (1994).
11 W. H. Pirkle and S. R. Selness, *J. Org. Chem.*, **60**, 3252 (1995).
12 Y. Kuroda, Y. Suzuki, J. He, T. Kawabata, A. Shibukawa, H. Wada, H. Fujima, Y. Go-oh, E. Imai, and T. Nakagawa, *J. Chem. Soc., Perkin Trans. 2*, **1995**, 1749.
13 K. B. Lipkowitz, "A Practical Approach to Chiral Separations by Liquid Chromatography," ed by G. Subramanian, VCH, New York (1994), Chap. 2.
14 K. B. Lipkowitz and A. G. Anderson, "Computational Approaches in Supramolecular Chemistry," ed by G. Wipff, Kluwer, Dordrecht (1994), p. 183.
15 K. B. Lipkowitz, *J. Chromatogr. A*, **694**, 15 (1995).
16 K. B. Lipkowitz, G. Pearl, B. Coner, and M. A. Peterson, *J. Am. Chem. Soc.*, **119**, 600 (1997).
17 K. B. Lipkowitz, R. Coner, and M. A. Peterson, *J. Am. Chem. Soc.*, **119**, 11269 (1997).
18 J. E. H. Köhler, M. Hohla, M. Richters, and W. A. König, *Angew. Chem., Int. Ed. Engl.*, **31**, 319 (1992).
19 K. B. Lipkowitz, D. A. Demeter, and C. A. Parish, *Anal. Chem.*, **59**, 1731 (1987).
20 K. B. Lipkowitz, D. A. Demeter, R. Zegarra, R. Larter, and T. Darden, *J. Am. Chem. Soc.*, **110**, 3446 (1988).
21 K. B. Lipkowitz and B. Baker, *Anal. Chem.*, **62**, 770 (1990).
22 W. H. Pirkle, J. A. Burke, III, and S. R. Wilson, *J. Am. Chem. Soc.*, **111**, 9222 (1989).
23 E. Francotte and G. Rihs, *Chirality*, **1**, 80 (1989).
24 Y. Okamoto, M. Kawashima, and K. Hatada, *J. Chromatogr.*, **363**, 173 (1986).
25 E. Yashima, M. Yamada, and Y. Okamoto, *Chem. Lett.*, **1994**, 579.
26 E. Yashima, M. Yamada, C. Yamamoto, M. Nakashima, and Y. Okamoto, *Enantiomer*, **2**, 225 (1997).
27 E. Yashima, C. Yamamoto, and Y. Okamoto, *J. Am. Chem. Soc.*, **118**, 4036 (1996).
28 B. R. Brooks, R. E. Bruccoleri, B. D. Olafson, D. J. States, S. Swaminathan, and M. Karplus, *J. Comput. Chem.*, **4**, 187 (1983).
29 F. A. Momany and R. Rone, *J. Comput. Chem.*, **13**, 888 (1992).
30 I. K. Roterman, M. H. Lambert, K. D. Gibson, and H. A. Scheraga, *J. Biomol. Struct. Dyn.*, **7**, 421 (1989).
31 "Quanta 4.0 Generating and Displaying Molecules," MSI.
32 S. L. Mayo, B. D. Olafson, and W. A. Goddard, III, *J. Phys. Chem.*, **94**, 8897 (1990).
33 "Cerius2 User's Reference Release 1.0," MSI.
34 H. Sun, *J. Comput. Chem.*, **15**, 752 (1994).
35 H. Sun, *Macromolecules*, **28**, 701 (1995).
36 H. Sun, S. J. Mumby, J. R. Maple, and A. T. Hagler, *J. Am. Chem. Soc.*, **116**, 2978 (1994).
37 "Discover 2.9.8/96.0/4.00 User Guide," MSI, 1996.
38 A. K. Rappé and W. A. Goddard, III, *J. Phys. Chem.*, **95**, 3358 (1991).
39 E. Yashima, M. Yamada, Y. Kaida, and Y. Okamoto, *J. Chromatogr. A*, **694**, 347 (1995).
40 P. J. Flory, "Principles of Polymer Chemistry," Cornell University Press, Ithaca, New York (1953).
41 C. F. Fan, B. D. Olafson, M. Blanco, and S. L. Hsu, *Macromolecules*, **25**, 3667 (1992).
42 "Cerius2 Computational Instruments User's Reference Release 1.5," MSI, Chap. 2.
43 "Polymer 4.00 User Guide Part 1," MSI, 1996.
44 M. Haisa, S. Kashino, and M. Morimoto, *Acta Crystallogr., Sect. B*, **36**, 2832 (1980).
45 F. H. Allen and O. Kennard, *Chem. Des. Autom. News*, **8**, 31 (1993).
46 U. Vogt and P. Zugenmaier, *Ber. Bunsenges. Phys. Chem.*, **89**, 1217 (1985).
47 D. N. Theodorou and U. W. Suter, *Macromolecules*, **18**, 1467 (1985).
48 H. Hopf, W. Grahn, D. G. Barrett, A. Gerdes, J. Hilmer, J. Hucker, Y. Okamoto, and Y. Kaida, *Chem. Ber.*, **123**, 841 (1990).
49 K. Maeda, Y. Okamoto, N. Morlender, N. Haddad, I. Eventove, S. E. Biali, and Z. Rappoport, *J. Am. Chem. Soc.*, **117**, 9686 (1995).
50 K. Maeda, Y. Okamoto, O. Toledano, D. Becker, S. E. Biali, and Z. Rappoport, *J. Org. Chem.*, **59**, 5473 (1994).